Influence of internal electric fields and surface charges on the transport of an optically generated electron-hole plasma

T. Held, T. Kuhn, and G. Mahler
Institut für Theoretische Physik, Universität Stuttgart, Pfaffenwaldring 57, D-7000 Stuttgart-80, Germany
(Received 8 July 1991)

A hydrodynamic description based on a heated displaced Maxwellian approximation is used to investigate the perpendicular transport of an electron-hole plasma, generated by a laser pulse in a thin semiconductor slab. Internal electric fields and surface charges are built up due to different bulk and surface properties of the two charge-carrier types. The response of the plasma is studied on different time and length scales in terms of hydrodynamic and electric variables. If the surface charges are small, the internal electric field is measurable as a small external voltage known as the Dember effect. In this regime, the field has practically no influence on the transport, and an ambipolar model can be applied for the calculation of the hydrodynamic variables. Large surface charges, however, lead to fields much stronger than the Dember field and limit the validity of the ambipolar approximation.

I. INTRODUCTION

The transport of optically generated electrons and holes in semiconductors has initially been investigated within the framework of steady-state problems in bulk samples.[1,2] New techniques in fabrication of microstructured and nanostructured samples and generation of short laser pulses allow one to study the carrier dynamics on short length and time scales. Various problems, like carrier cooling,[3] transport in systems with reduced dimensionality,[4–8] carrier capture in quantum wells,[9] or influence of surface fields,[10] are of actual interest.

The theoretical model used to explain the measured results for a given experiment depends not only on the sample geometry but also on the details of the experimental conditions. The excitation with low laser energy and power density generates only a few quasithermalized carriers that do not form an electron-hole plasma but an exciton gas. Then transport can be explained in terms of isothermal diffusion.[5,7] In other cases, especially if high energies and power densities are used, it is necessary to take into account additional degrees of freedom, like the carrier temperature[3] or hot phonons.[11] Common methods are either a direct integration of the transport equations[12] or Monte Carlo techniques.[11] While the former is appropriate to get the whole distribution function, the latter provides primarily its moments.

In the plasma case electrons and holes do not necessarily remain together after generation, but, due to different masses and mobilities, diffuse apart and build up space charges and thus internal electric fields. This phenomenon, the so-called Dember effect,[15] leads to an externally measurable voltage, the transverse photovoltage.[2] But the internal field reacts on the carriers, reducing the diffusion of the light carriers by a backward-directed drift and accelerating the heavy ones. In case of a strong coupling the carriers form a new effective particle fluid with a local charge neutrality on length scales larger than the Debye length, and the so-called ambipolar approximation can be applied. We previously have used this approach to investigate the perpendicular transport of an inhomogeneously generated ambipolar electron-hole plasma in a semiconductor slab.[13,14]

An analogue to the Dember effect is given in the case of carrier capture in and emission from quantum wells[9,16] or at surface states. A typical experiment[9] is to generate carriers in a quantum well ($In_{1-x}Ga_xAs/InP$) by using a laser energy smaller than the barrier gap. Due to a small activation energy the electrons may leave the quantum well and move into the bulk while the holes remain in the well. The diffusion of the electrons is then hindered by the increasing electric field.

Quite contrary to an ambipolar behavior is the functioning of a photodiode: here, the charge carriers are separated by an intentionally built-in field due to the band structure, a phenomenon which is not the subject of this paper.

In the present contribution we will investigate the deviations from local charge neutrality and effects of internal fields. Then, by comparing the results with those obtained within the ambipolar model, we will estimate the validity and the limitation of the latter approximation. Section II introduces the model and scenario we use. In Sec. III some simulations for the spatial and temporal evolution of hydrodynamic and electric quantities in the bulk are presented. The influence of different surface parameters is studied in Sec. IV. Finally, some conclusions are drawn in Sec. V.

II. THE MODEL

We investigate a semiconductor sample, which is confined in one direction (the z direction, width L) and has large extensions in the two lateral directions. A simplified band structure with a direct gap and two parabolic bands is assumed. The surface at $z=0$ is perpendicularly illuminated by a monochromatic defocused laser with time-dependent intensity. Entering the crystal, the

laser beam generates electron-hole pairs with an excess energy depending on the laser frequency and with a spatial distribution due to an exponential absorption. Carrier transport is induced by density and temperature gradients. Scattering events of the carriers among themselves and with phonons, impurities, and disorder lead to relaxation of momentum and energy of the carriers. Finally, surface recombination is taken into account, which is assumed to be large compared to bulk recombination. For the simulation the material parameters of $Ga_{0.8}Al_{0.2}As$ are used.

In a kinetic description an electron-hole plasma is characterized by two Boltzmann equations for the distribution functions f_c for electrons ($c=e$) and holes ($c=h$), respectively, and, due to the charge of the carriers, by a Poisson-equation for the electric field **E**. We assume that the phonons remain in equilibrium and take them into account as a heat bath only. Due to the lateral homogeneous excitation the distribution functions have a one-dimensional space dependence, and the electric field vector has a single component, E_z. In velocity space a full three-dimensional dependence on the carrier velocity, **v**, is considered. Thus we have

$$\frac{\partial}{\partial t}f_c(z,\mathbf{v},t)+v_z\frac{\partial}{\partial z}f_c(z,\mathbf{v},t)+\frac{q_cE_z}{m_c}\frac{\partial}{\partial v_z}f_c(z,\mathbf{v},t) =g_c(z,\mathbf{v},t)+\left[\frac{\partial f}{\partial t}\right]_c^{\text{coll}}, \quad c=e,h \ , \tag{1}$$

$$\frac{\partial}{\partial z}E_z=\frac{e}{\epsilon_0\epsilon_r}(n_h-n_e+N_D^+-N_A^-) \ . \tag{2}$$

Here, n_c is the density of carrier-type $c=e$, h, N_D^+ and N_A^- the densities of ionized impurities, $q_e=-e$ and $q_h=+e$ the charges, m_c the effective carrier mass, and ϵ_r the background dielectric function. The generation term g_c is proportional to the laser power density and has an exponential spatial dependence. Finally, the collision term consists of three parts: (i) electron-electron and hole-hole; (ii) electron-hole; and (iii) carrier-lattice scattering (scattering with phonons, impurities, and alloy scattering).

For a carrier-carrier scattering rate large compared with the carrier-lattice scattering rate, the distribution functions are approximately heated displaced Maxwellians. In a previous paper[12] we have already investigated the validity of this hydrodynamic approach for a stationary scenario of the problem. But also in the case of pulses,[14] when the density raises from an equilibrium value up to its maximum, the calculated carrier-carrier scattering rates[17] fulfill the hydrodynamic condition. The first three moments of the distribution function determine the carrier densities n_c, the drift velocities v_c, and the carrier temperatures T_c, expressed by $\Theta_c=k_BT_c/m_c$:

$$n_c(z,t)=\frac{1}{4\pi^3}\int f_c(z,\mathbf{v},t)d^3v \ ; \tag{3}$$

$$v_c(z,t)\mathbf{e}_z=\frac{1}{n_c(z,t)}\frac{1}{4\pi^3}\int \mathbf{v}f_c(z,\mathbf{v},t)d^3v \ ; \tag{4}$$

$$\Theta_c(z,t)=\frac{1}{3n_c(z,t)}\frac{1}{4\pi^3}\int[\mathbf{v}-v_c(z,t)\mathbf{e}_z]^2f_c(z,\mathbf{v},t)d^3v \ ; \tag{5}$$

where $\mathbf{e}_z$ is the unit vector in the z direction. These three moments, called the hydrodynamic variables, characterize the respective heated displaced Maxwellian (HDM),

$$f_c^{\text{HDM}}(z,\mathbf{v},t)=\frac{n_c(z,t)}{2}\left[\frac{2\pi}{\Theta_c(z,t)}\right]^{3/2} \times\exp\left[-\frac{[\mathbf{v}-v_c(z,t)\mathbf{e}_z]^2}{2\Theta_c(z,t)}\right] . \tag{6}$$

Inserting the HDM (6) into the Boltzmann equation (1) and forming the three moments in analogy to Eqs. (3)–(5) we get six nonlinear hydrodynamic equations,

$$\frac{\partial}{\partial t}n_c+\frac{\partial}{\partial z}n_cv_c=G^{(0)} \ , \tag{7}$$

$$\frac{\partial}{\partial t}v_c+\frac{\Theta_c}{n_c}\frac{\partial}{\partial z}n_c+v_c\frac{\partial}{\partial z}v_c+\frac{\partial}{\partial z}\Theta_c-\frac{q_cE_z}{m_c} =\frac{1}{n_c}(J_c^{(1)}-v_cG^{(0)}) \ , \tag{8}$$

$$\frac{\partial}{\partial t}\Theta_c+\frac{2}{3}\Theta_c\frac{\partial}{\partial z}v_c+v_c\frac{\partial}{\partial z}\Theta_c =\frac{1}{3n_c}(J_c^{(2)}+G_c^{(2)}-3\Theta_cG^{(0)}), \quad c=e,h \ . \tag{9}$$

The $G_c^{(\nu)}$ and $J_c^{(\nu)}$ are the νth moments of the generation term and the collision term, respectively. They are defined in Appendix A.

The model for the boundary depends on the technological realization of the slab: For pure bulk effects a very thick slab is sufficient,[1] and no special boundary model is needed. Slabs of a width of several micrometers[4] may have two free surfaces. However, a slab a few micrometers wide can only be grown on a substrate, thus having one free surface and one interface to the substrate. Then, three limiting cases can be distinguished: (i) the substrate has a larger gap than the slab and acts as a potential barrier for the carriers; (ii) the substrate has a very small conductivity and the carriers remain close to the interface; (iii) the substrate has a very high conductivity and a large extension and the carriers spread out into the substrate. In all three cases the carrier density in the substrate (and thus space charges) will approximately vanish: the interface acts an an effective surface, and for simplicity we will also call it a surface. Due to dangling bonds, lattice mismatch or other technological reasons, the surfaces provide a certain number of bound states for the carriers.

Various surface models for kinetic and hydrodynamic boundary conditions have been discussed in Refs. 16 and 18. A particle reaching the surface is either reflected or captured in a bound state, where it can recombine with the other carrier type. If the surface is an effective one as described above, the capturing also contains the

transmission of the particle through the (inter)face. In the hydrodynamic model the properties of the surface are described by surface recombination velocities for electrons and holes

$$s_c(0)=-j_c/(n_c-n_c^{(0)})|_{z=0}\ ,$$
$$s_c(L)=j_c/(n_c-n_c^{(0)})|_{z=L}\ ,\quad c=e,h\ . \tag{10}$$

Here, $j_c=n_c v_c$ is the particle current density, and $n_c^{(0)}$ is an equilibrium density (see Appendix C). The values for s_c specifying certain interaction mechanisms between carriers and surface are discussed in Sec. IV.

The capture of a carrier by a surface state is, in our model, the first step of a recombination, which reduces the number of electrons and holes in the surface states pairwise. Different surface recombination velocities imply a different occupation of these states, and thus a surface charge σ is built up. For this quantity we get after integrating a simple charge continuity equation

$$\frac{\partial}{\partial t}\sigma(0)=e(j_e-j_h)|_{z=0}\ ,$$
$$\frac{\partial}{\partial t}\sigma(L)=e(j_h-j_e)|_{z=L}\ . \tag{11}$$

The surface charge is directly connected with the difference of the electric field across the boundary by the equation

$$\sigma(0)=\epsilon_0\epsilon_r E_z|_{z=0},\quad \sigma(L)=-\epsilon_0\epsilon_r E_z|_{z=L}\ . \tag{12}$$

This equation acts as a boundary condition for the electric field. The remaining boundary conditions are listed in Appendix B.

Our scenario will be the following: All the simulations start from thermal equilibrium (see Appendix C). The laser excitation is a single Gaussian pulse with a width t_w centered at $t=0$ (see Appendix A). The response of the sample is described in terms of the hydrodynamic and electric variables.

III. NONEQUILIBRIUM IN BULK

In this section we study the influence of the electric field and, by Poisson equation (2), its derivative, the electric charge density. To get mainly bulk properties and reduce the influence of the surfaces to a minimum, we choose equal surface recombination velocities for both carrier types at both surfaces in this section. The next section will justify this choice.

Due to quite different masses electrons and holes tend to move independently, but they are coupled by the internal electric field. The strength of this coupling is now investigated. In Fig. 1 two simulations of Eqs. (7)–(9) with different laser power densities are compared with each other. Instead of an absolute density the difference between the density and the equilibrium value normalized to the maximum of the corresponding hole densities is plotted. We recognize that in the higher power case the densities and velocities are nearly identical, while in the other case the electrons reach a drift velocity one order of magnitude larger, due to small restoring forces, and the density raises outside the generation region. Apart from screening, Eqs. (7)–(9) scale with the laser power while Eq. (2) depends on absolute densities. Therefore, the influence of an internal electric field comes more and more into play with increasing density.[18] Another fact is observed from Fig. 1. Even in the case of small coupling the holes behave nearly as they do in the strongly coupled case, which means that the ambipolar transport is dominated by the holes: The formula for the ambipolar diffusion constant[18] expresses this, $D^{-1}=(D_e^{-1}+D_h^{-1})/2$. The densities reached in the low power simulation are of the order of the equilibrium values. Thus the excess energy of newly generated carriers is also supplied to heat the cold equilibrium carriers and the carrier temperatures cannot reach the values of the high power simulation (the step in the electron temperature curve is due to a nearly vanishing excess density).

The ambipolar approximation is based on the assumption that the local densities of electrons and holes are equal due to electric forces, which means that the charge density is vanishing. Therefore, a good measure for the

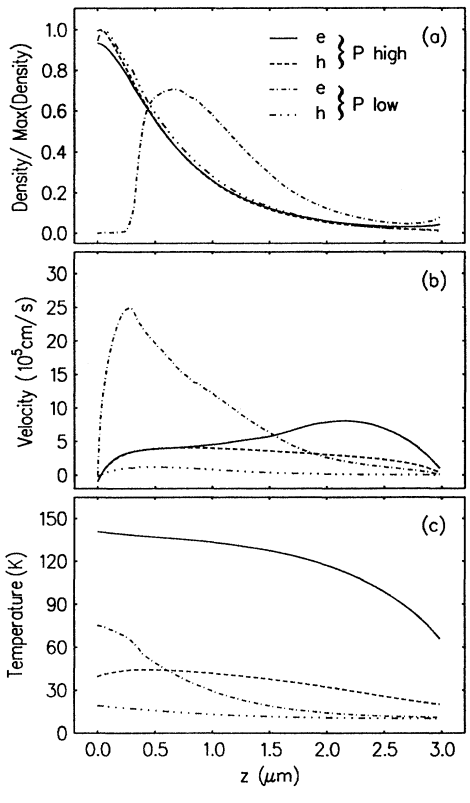

FIG. 1. Spatial profiles at $t=-t_w/2$ of the density, (a), drift (b), and temperature, (c), of electrons and holes for two different laser power densities. Solid and dashed line: $\bar{P}=2$ W mm^{-2}, maximum density 1.5×10^{15} cm^{-3}; dashed-dotted and dashed-triple-dotted line: $\bar{P}=0.02$ W mm^{-2}, maximum density 1.2×10^{13} cm^{-3}. Remaining parameters: $T_L=10$ K, $s_c=10^5$ cm/s, $N_D=7\times10^{13}$ cm^{-3}, $N_A=3\times10^{13}$ cm^{-3}, $t_w=20$ ps, $E_{\rm exc}=75$ meV.

validity of this assumption is the difference between electron and hole densities, Δn. In Fig. 2 we see the temporal evaluation of this quantity (divided by the arithmetic mean of both, $\bar{n}$) at different positions in the sample. The carriers are generated in a region less then half a micrometer away from the illuminated surface. Then, due to their smaller mass, the electrons move faster out of this region than the holes. The first curve ($z=0.25$ μm) shows the dominance of the holes after some electrons have left the generation region. On the other hand, the curves with $z=1.5$ μm and $z=2.75$ μm demonstrate that the electron density is now larger than that of the holes, due to the transport into the rest of the sample. The second curve ($z=0.5$ μm) is approximately in the boundary region of the generation region and shows a superposition of both processes. In the beginning the electron density increases due to the incoming transport from the greater part of the generation region, but then the electrons keep on moving into the rest of the sample and the hole density dominates. Transport is also responsible for the maximum of the fourth curve ($z=2.75$ μm) appearing retarded compared to the third curve ($z=1.5$ μm) which is only half the distance away from the generation region. In any case, the maximum value of Δn is about 20–30 % of $\bar{n}$. This seems to be substantial; however, these peaks are at a time (beginning of leading edge of the pulse) and in a region (far away from the generation region) where the density is still small: The absolute local density differences are negligible in all phases of the simulation for these special boundary conditions.

The influence of electric quantities on transport is given by the term of the electric field in Eq. (8). As a measure for this influence we choose the internal field strength. This quantity can be reduced by screening effects and "compensation transport." Compensation transport means that regions with a space charge of different sign exchange mobile charge carriers by transport until the charges are reduced to a minimum. In Fig. 3 we show the electric field at $t=-t_w$. The solid curve corresponds to the simulations as of Fig. 2. We recognize a rapidly increasing field (excess of holes) in the generation region and a decreasing field in the rest of the sample

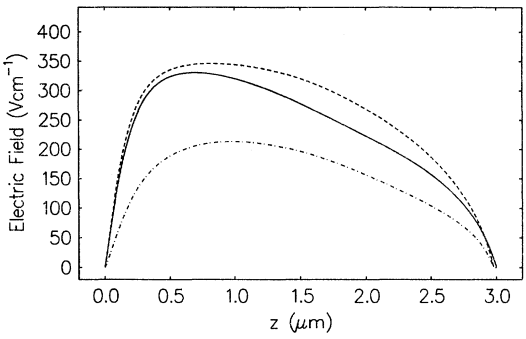

FIG. 3. Electric field at $t=-t_w/2$. Excitation by three different pulses: $t_w=20$ ps and $E_{\rm exc}=75$ meV (solid line), $t_w=20$ ps and $E_{\rm exc}=125$ meV (dashed line), $t_w=100$ ps and $E_{\rm exc}=75$ meV (dashed-dotted line). Other parameters as in Fig. 2.

(excess of electrons). The field has its maximum in the generation region because a high carrier temperature there reduces the screening of the carriers. Furthermore we notice a nearly vanishing field at the boundaries indicating a vanishing surface charge [see Eq. (12)] due to equal surface recombination velocities for both carrier types. This and the influence of a substantial surface charge will be discussed in the next section. Compared to the 75-meV curve, the 125-meV curve has a higher field everywhere because a larger excess energy implies a larger carrier temperature and thus a reduced screening. On the other hand a larger pulse width (100 ps instead of 20 ps) reduces the electric field: The carriers have more time to compensate local charge accumulation by transport.

The electric potential, the integral of the field, is not explicitly contained in the transport equations, but as voltage between the two surfaces it is a measurable quantity. The fact that such a voltage appears due to internal electric fields, is called the Dember effect.[1,15] In Fig. 4 we see the temporal evolution of this voltage. The influence of different excess energies and different pulse widths on

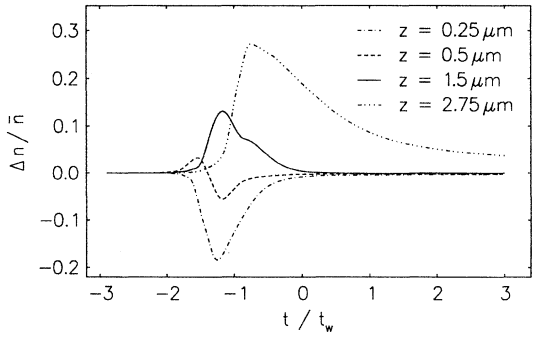

FIG. 2. Temporal evolution of the difference of electron and hole densities, Δn, with respect to their arithmetic mean $\bar{n}$ at several positions in the sample. $\bar{P}=2$ W mm^{-2}, other parameters as in Fig. 1.

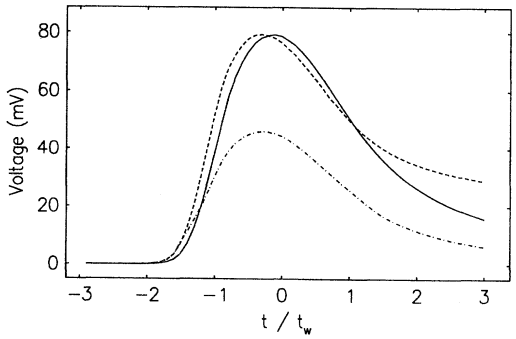

FIG. 4. Temporal evolution of the voltage between the two surfaces (Dember effect). Parameters and line types as in Fig. 3.

the amplitudes is the same as in the case of the electric field. The maximum voltage occurs at a time between the turning point and the maximum of the laser pulse. This confirms that the nonequilibrium has its greatest influence at the leading edge of the laser pulse.

IV. INFLUENCE OF SURFACE PARAMETERS

The surface recombination velocity contains all mechanisms describing the interaction between a carrier and the surface. In realistic samples the capture by surface states is a process more important for holes than for electrons. Furthermore the density of states is usually larger at a free surface ($z=0$) than at an effective surface (interface to the substrate, $z=L$). The transition through an interface depends on the value of the band discontinuity of the two adjacent regions. A substrate with a smaller bandgap (GaAs) than those of the slab often leads to higher surface recombination velocities than a substrate made, e.g., of AlAs. The surface models[16,18] show that the transition through an interface is proportional to the thermal velocity of the carrier. Due to a higher temperature and a smaller mass the electrons have a larger transition probability.

With the four surface recombination velocities (electrons and holes, respectively, and boundary at $z=0$ and L) a vast spectrum of parameters and scenarios is covered. From all these possible combinations we now investigate the three most important ones. Case a: The four velocities are equal, which means that capturing in surface states at $z=0$ is of the same order of magnitude as the sum of transition and capturing at $z=L$, and the effect of a higher thermal velocity of the electrons is compensated by a higher density of surface states for the holes. This case has already been simulated in the last section. Here it is used as reference for the other two cases. Case b: At $z=0$ the hole velocity is more than one order of magnitude larger than that of the electrons (strong capture of holes in surface states), at $z=L$ the situation is like case a. Case c: At $z=0$ it is like case b, at $z=L$ the electrons have a larger velocity than the holes (strong transition of electrons into the substrate).

The voltage between the two surfaces is a superposition of two contributions, the voltage due to the surface charges and their screening charges, and the Dember voltage (as described in the previous section) due to nonambipolar diffusion in the bulk. In Fig. 5 the temporal evolution of this total voltage is plotted; in Fig. 6 we see the electric field profile at $t=t_w$. The electrical quantities of case a are dominated by the Dember effect. Surface charges are small. Case b behaves like case a until the pulse maximum, but then the Dember effect loses its dominant role: The strong capturing of holes in surface states at $z=0$ builds up a large surface charge which is not vanishing in the relaxation phase of the system (Fig. 5). This means that also in thermal equilibrium a surface charge will remain which is even more important than the Dember-effect. The electric field (Fig. 6) of case b and its gradient show at $z=0$ a positive surface charge, followed by a negative space charge for screening, while at $z=L$ electric field (and surface charge) are nearly vanishing. Near $z=0$ the electric field (Fig. 6) of case c behaves like case b, but, due to surface recombination velocities being of the same order, the (positive) surface charge is smaller. At $z=L$ a negative surface charge and a positive space charge are built up. These charges have to be transported through the slab by the carriers. Due to this delay the charges do not yet have their steady-state value at the end of the laser pulse, and the voltage (Fig. 5) for case c is still increasing. For case b with a small final charge at $z=L$ the delay due to transport is negligible, and the voltage has reached its steady-state value. We also see that Dember effect is no longer important for case c.

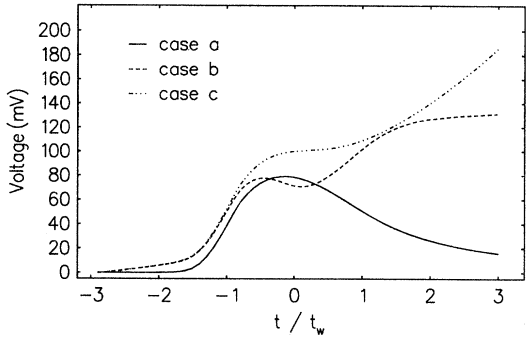

FIG. 5. Temporal evolution of the voltage between the two surfaces. Surface recombination velocities: case a, $s_e(0)=s_h(0)=s_e(L)=s_h(L)=10^5$ cm/s; case b, $s_e(0)=5\times10^4$ cm/s, $s_h(0)=8\times10^5$ cm/s, $s_e(L)=s_h(L)=2\times10^5$ cm/s; case c, $s_e(0)=2\times10^4$ cm/s, $s_e(L)=2\times10^5$ cm/s, $s_h(0)=s_h(L)=8\times10^4$ cm/s. Other parameters as in Fig. 2.

The change of voltage and surface charges by a laser pulse has also been observed experimentally:[10] there, a GaAs sample has been investigated within a pump-and-probe experiment by time-resolved reflective electro-optic sampling. The evolution of the reflection coefficient demonstrates the strong electrical field changes.

Finally, we come back to the ambipolar approximation. If the surface charge, and in consequence the compensation (screening) space charge near the surface, are large (Fig. 6), the difference of the densities of the two

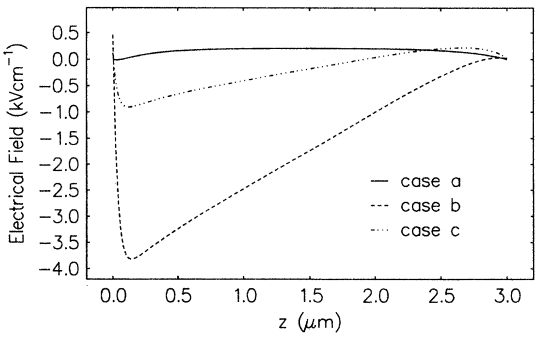

FIG. 6. Spatial profiles of the electric field at $t=t_w$. Parameters and line types as in Fig. 5.

carrier types will be so distinct that an ambipolar model cannot be used. However, if the slab is thick enough, this approach might be applied in the bulk far away from the surfaces.

V. CONCLUSIONS

The numerical simulations of an electron-hole plasma, which is generated and heated inhomogeneously in space and time, demonstrate that a description with the assumption of local neutrality, the so-called ambipolar description, is a very good approximation on all relevant scales provided the influence of surface charges is small. The Dember effect describing the formation of a voltage amounts to a measurable but small quantity. It has its maximum at the leading edge of the laser pulse. The effect is reduced by compensation transport in case of large pulses and enhanced by high carrier temperatures. Quite different surface recombination velocities for electrons and holes support the buildup of surface charges. The voltage induced by these charges and their compensation space charges in bulk may even exceed the Dember effect: then the ambipolar model looses its applicability.

ACKNOWLEDGMENTS

The authors would like to thank K. Scheller for valuable discussions. This work has been supported by the Deutsche Forschungsgemeinschaft (Bonn, Germany) under Grant No. Ma-614/5-2.

APPENDIX A

In the system of hydrodynamic equations (7)–(9) we have used the following abbreviations for the moments of the generation and the collision term:

$$G^{(0)}=\frac{1}{4\pi^3}\int g_e(z,\mathbf{v},t)d^3v$$
$$=\frac{1}{4\pi^3}\int g_h(z,\mathbf{v},t)d^3v=\frac{\alpha P(t)}{\hbar\omega_L}e^{-\alpha z},$$

$$G_c^{(2)}=\frac{1}{4\pi^3}\int[\mathbf{v}-v_c(z,t)\mathbf{e}_z]^2 g_c(z,\mathbf{v},t)d^3v$$
$$=G^{(0)}\left[\frac{2E_{\rm exc}}{(1/m_e+1/m_h)m_c^2}+v_c^2\right],$$

$$J_c^{(1)}\mathbf{e}_z=\frac{1}{4\pi^3}\int\mathbf{v}\left[\frac{\partial f}{\partial t}\right]_c^{\rm coll}d^3v,$$

$$J_c^{(2)}=\frac{1}{4\pi^3}\int[\mathbf{v}-v_c(z,t)\mathbf{e}_z]^2\left[\frac{\partial f}{\partial t}\right]_c^{\rm coll}d^3v.$$

$P(t)$ is the laser power density, α^{-1} the absorption length, $\hbar\omega_L$ the photon energy, and $E_{\rm exc}$ the excess energy. For our scenario we have chosen a Gaussian laser pulse

$$P(t)=(2/\pi)^{1/2}\bar{P}(t_r/t_w)\exp[-2(t/t_w)^2],$$

where $\bar{P}$ is an average power density and t_r a pulse repetition time of 1000 ps.

The derivation of the collision term and its moments $J^{(v)}$ has already been published in Ref. [13]. The moments can be divided into two parts: the electron-hole scattering and the carrier-lattice scattering. Scattering times, depending nonlinearly on the hydrodynamic variables, are defined by

$$J_c^{(1)}=-n_c(v_c-v_{c'})\frac{1}{\tau_{c(eh)}^{(1)}}-n_c v_c\sum_i\frac{1}{\tau_{c(i)}^{(1)}},$$

$$J_c^{(2)}=-n_c\frac{3k_B}{m_c}(T_c-T_{c'})\frac{1}{\tau_{c(eh)}^{(2)}}$$
$$-n_c\frac{3k_B}{m_c}(T_c-T_L)\sum_i\frac{1}{\tau_{c(i)}^{(2)}}-2v_cJ_c^{(1)},$$

$$c,c'=e,h;\ c\neq c,$$

where T_L means lattice temperature and the sum indicates summation over the various carrier-lattice scattering mechanisms. For the latter we refer to Ref. [13]. The electron-hole scattering times are

$$\frac{1}{\tau_{c(\rm eh)}^{(1)}}=n_{c'}m_{c'}\left[2\pi k_B\left[\frac{T_e}{m_e}+\frac{T_h}{m_h}\right]\right]^{-3/2}\frac{2}{3}\frac{m_e+m_h}{(m_em_h)^2}$$
$$\times\left[\frac{e^2}{\epsilon_0\epsilon_r}\right]^2\int_0^\infty\frac{\xi^3e^{-\xi^2/2}}{(\xi^2+\Lambda^{-2})^2}d\xi,$$

$$\frac{1}{\tau_{c(\rm eh)}^{(2)}}=\frac{1}{\tau_{c(\rm eh)}^{(1)}}\frac{m_c}{m_e+m_h},$$

with

$$\Lambda^{-2}=\lambda^{-2}\frac{\hbar^2}{4k_B}\left[\frac{1}{m_e}+\frac{1}{m_h}\right]^2\left[\frac{T_e}{m_e}+\frac{T_h}{m_h}\right]^{-1},$$

and

$$\lambda^{-2}=\frac{e^2}{\epsilon_0\epsilon_r k_B}\left[\frac{n_e}{T_e}+\frac{n_h}{T_h}\right].$$

APPENDIX B

To get boundary conditions for Eqs. (7)–(9) we express v_c and Θ_c by the variables $j_c=n_cv_c$ and $b_c=n_c^{-2}\Theta_c$ and transform the equation system to these new variables. The result is

$$\frac{\partial}{\partial t}n_c+\frac{\partial}{\partial z}j_c=G^{(0)},$$

$$\frac{\partial}{\partial t}j_c+\left[\frac{5}{3}b_cn_c^{2/3}-\left[\frac{j_c}{n_c}\right]^2\right]\frac{\partial}{\partial z}n_c+\frac{2j_c}{n_c}\frac{\partial}{\partial z}j_c$$
$$+n_c^{5/3}\frac{\partial}{\partial z}b_c-n_c\frac{q_cE_z}{m_c}=J_c^{(1)},$$

$$\frac{\partial}{\partial t}b_c+\frac{j_c}{n_c}\frac{\partial}{\partial z}b_c=\frac{1}{3}n_c^{-5/3}(J_c^{(2)}+G_c^{(2)}-3n_c^{2/3}b_cG^{(0)}),$$

$$c=e,h.$$

The common boundary conditions for the first two equa-

tions are Eqs. (10). For $j_c=0$ the third equation becomes an ordinary differential equation, which is integrable with an initial condition and thus serves as spatial boundary condition.

APPENDIX C

Our simulation starts from thermal equilibrium, and thus fixing the initial conditions for the differential equation system: Carriers and lattice have the same temperature, and the drift velocities are vanishing. In the bulk the carrier densities are determined by thermal band-band generation and ionization of impurities. We denoted these densities $n_c^{(0)}|_b$. Close to the surfaces a few carriers are captured in bound states and leave ionized impurities in the slab until an electric field is built up. This phenomenon can be considered either as an equilibrium between a drift and a diffusion current or as a bending of the bands due to a Fermi-level pinning. If this bending is small compared to $k_B T_L$, the Poisson equation (2) can be expanded, and electric potential and field are decaying exponentially in terms of a Debye length λ_s. Using Eq. (12) we obtain

$$n_c^{(0)}(z)=n_c^{(0)}|_b\left\{1-\frac{q_c\lambda_s}{\epsilon_0\epsilon_r k_B T_l}\left[\sigma^{(0)}(0)\exp\left[-\frac{z}{\lambda_s}\right]+\sigma^{(0)}(L)\exp\left[\frac{z-L}{\lambda_s}\right]\right]\right\},$$

with

$$\lambda_s^{-2}=\frac{e^2}{\epsilon_0\epsilon_r k_B T_L}(n_e^{(0)}|_b+n_h^{(0)}|_b)\ .$$

The resulting densities at the surfaces also enter Eq. (10).

To get a relation between equilibrium surface charge and surface recombination velocity we consider the following picture: some carriers (mainly the part of $n_h^{(0)}|_b$ due to ionization of impurities) move toward the surface until the density has dropped to the value due to thermal band-band generation, which we will call $n_{\rm th}$. The time for this process is available from the width of the region of this density change, approximately λ_s, and the average carrier velocity being in the order of their surface recombination velocity. Using Eq. (10) and integrating Eq. (11) formally we get the ansatz.

$$\sigma^{(0)}=e[(n_h^{(0)}|_b-n_{\rm th})s_h-(n_e^{(0)}|_b-n_{\rm th})s_e]\frac{\lambda_s}{(s_e+s_h)/2}\ .$$

The equilibrium state is calculated by a simulation without laser excitation and under steady-state conditions.

[1]H. Dember, Phys. Z **32**, 554 (1931); **33**, 207 (1932).
[2]R. A. Smith, *Semiconductors* (Cambridge University Press, Cambridge, 1961), p. 313.
[3]J. Shah, Superlatt. Microstruct. **6**, 293 (1989).
[4]H. Hillmer, T. Kuhn, B. Laurich, A. Forchel, and G. Mahler, Phys. Scr. **35**, 520 (1987).
[5]H. Hillmer, A. Forchel, S. Hansmann, M. Morohashi, E. Lopez, H. P. Meier, and K. Ploog, Phys. Rev. B **39**, 10 901 (1989).
[6]K. T. Tsen, G. Halama, O. F. Sankey, S.-C. Y. Tsen, and H. Morkoc, Phys. Rev. B **40**, 8103 (1989).
[7]A. Forchel, B. E. Maile, H. Leier, G. Mayer, and R. Germann, Phys. Status Solidi **159**, 457 (1990).
[8]D. Ahn, J. Appl. Phys. **69**, 3596 (1991).
[9]U. Cebulla, G. Bacher, A. Forchel, S. Schmitz, H. Jürgensen, and M. Razeghi, Appl. Phys. Lett. **55**, 933 (1989).
[10]W. Kütt, G. C. Cho, M. Strahnen, and H. Kurz (in press).
[11]P. Lugli, P. Bordone, L. Reggiani, M. Rieger, P. Kocevar, and S. M. Goodnick, Phys. Rev. B **39**, 7852 (1989).
[12]T. Kuhn and G. Mahler, Phys. Rev. B **39**, 1194 (1989).
[13]T. Held, T. Kuhn, and G. Mahler, Phys. Rev. B **41**, 5144 (1990).
[14]T. Held, T. Kuhn, and G. Mahler, Phys. Rev. B **42**, 11 934 (1990).
[15]K. Seeger, *Semiconductor Physics* (Springer, Berlin, 1973), p. 155.
[16]T. Kuhn and G. Mahler, Solid-State Electron. **32**, 1851 (1989).
[17]S. M. Goodnick and P. Lugli, Phys. Rev. B **37**, 2578 (1988).
[18]T. Kuhn and G. Mahler, Phys. Rev. B **40**, 12 147 (1989).